*Geophys. J. Int.* (2003) **154,** 134–145

# Analysis of broad-band regional waveforms of the 1996 September 29 earthquake at Bárdarbunga volcano, central Iceland: investigation of the magma injection hypothesis

Konstantinos I. Konstantinou,[1] Honn Kao,[2] Cheng-Horng Lin[1] and Wen-Tzong Liang[1]

[1] *Institute of Earth Sciences, Academia Sinica,* PO Box 1-55, *Nankang Taipei,* 115 *Taiwan, ROC. E-mail: lin@earth.sinica.edu.tw*
[2] *Geological Survey of Canada, Pacific Geoscience Centre,* 9860 *West Saanich Road,* PO Box 6000 *Sidney, British Columbia, Canada* V8L 4B2

Accepted 2003 January 30. Received 2002 December 17; in original form 2002 July 8



## SUMMARY

Large earthquakes near active volcanoes, that exhibit non-double-couple source properties are usually interpreted as the result of either magma intrusion or geometrical complexity along the fault plane. Such an earthquake occurred in 1996 September 29 at Bárdarbunga volcano in central Iceland, to be followed 2 days later by a major volcanic eruption at the area between Bárdarbunga and the nearby Grimsvötn volcano. Both of these active volcanic centres lie underneath the Vatnajökull glacier, a permanent ice cap that covers a large area of central Iceland. This event was recorded by a temporary network (HOTSPOT) that consisted of 30 broad-band three-component seismometers covering most of Iceland. The waveforms of this event at all stations show an emergent, low-amplitude, high-frequency onset that is superposed on a longer-period signal. The corresponding amplitude spectra show a low-frequency content ($<$1 Hz) and prominent peaks around the corner frequency ($\sim$0.25 Hz) and higher frequencies. These regional waveforms were inverted in order to obtain the best-fitting deviatoric and full moment tensor using a linear, time-domain inversion method. The results for the deviatoric moment tensor indicate a large ($\sim$60 per cent) compensated linear vector dipole (CLVD) component, a hypocentral depth of 3.5 km, a moment magnitude of 5.4 and a best double-couple solution showing thrust motion in good agreement with the previously published Harvard CMT solution. The results for the full moment tensor on the other hand, indicate an implosive isotropic component of 8.5 per cent, a reduced CLVD component of 47.2 per cent and a best double-couple solution showing normal faulting. However, a statistical F-test revealed that the full moment tensor does not fit the data significantly better than the deviatoric at a confidence level of not more than 76 per cent. All of these results were found not to change substantially when a different source time function was used or when the data were weighted according to their distance from the source. The data are consistent with an earthquake of this magnitude, caused by the failure of an asperity and the formation of a tensile crack due to increasing fluid pressure. The dimensions of the crack may have been $10 \times 3$ km$^2$ and 0.5 m thickness and the volume of the injected fluid was found to be $15 \times 10^6$ m$^3$. The calculated viscosity for the fluid (0.04 Pa s) points to the possibility of water being injected rather than magma, that is also supported by the short source duration of the earthquake ($\sim$5 s). Taking into account the water saturation of the upper crust in Vatnajökull due to the presence of the glacier, this event may have been caused by increased pressure of water that was heated by magma injected through a dyke below the asperity.

**Key words:** Bárdarbunga, dyke, Iceland, magma injection, moment tensor, non-double-couple.

## 1 INTRODUCTION

Earthquakes occurring near active volcanoes usually have small magnitudes ($M_w \sim$ 1–3) and are caused either by stresses induced by the ascent of magma to the Earth's surface or by the direct interaction of magma with its surrounding medium that results in the formation of tensile cracks (McNutt 1996). Larger earthquakes ($M_w \geq 5.0$) caused by the latter kind of interaction are rare events

**Table 1.** Reported observations of earthquakes directly related to magma flow/injection.

| Area | Depth | Magnitude | Process | Reference |
|---|---|---|---|---|
| Izu-Oshima, Japan | 30 km | 2.7 ($M_L$) | Traction force on conduit walls due to magma flow | Ukawa & Ohtake (1987) |
| Ito-Oki, Japan | 5 km | 5.5 ($M_L$) | Asperity rupture due to magma injection | Oura *et al.* (1992); Takeo (1992) |
| Tori-Shima, Japan | 10 km | 5.5 ($M_s$) | Magma/superheated water injection | Kanamori *et al.* (1993) |
| Kamchatka, Russia | 10 km | 6.6 ($M_s$) | Asperity rupture due to magma injection | Zobin & Levina (1998) |
| Tori-Shima, Japan | 24 km | 5.7 ($M_s$) | Magma injection | Sugioka *et al.* (2000) |

and in most cases have an estimated recurrence time of more than 100 years for a particular volcano (Zobin 2001). The study of such events is of great importance not only from the viewpoint of seismic hazard mitigation but also from the point of their source physics. Since the dominant source process of such events involves the opening and filling of tensile cracks with fluid (rather than just shearing motion along two fault blocks), the conventional double-couple force model cannot describe them adequately (Julian *et al.* 1998). Therefore, a more plausible model in terms of an equivalent force system acting at the source is the compensated linear vector dipole (CLVD) (Ishimoto 1932; Knopoff & Randall 1970).

There are several examples of such large earthquakes in volcanic areas caused by tensile cracking due to fluid–rock interaction (Table 1). Most of them had distinct characteristics that made them easily discernible from events of purely tectonic origin. Some of these characteristics included: an almost monochromatic low-frequency content of the waveform (Ukawa & Ohtake 1987); generation of disproportionately large tsunamis and absence of any Love waves from the radiated wavefield (Kanamori *et al.* 1993); and continuous migration of aftershocks towards the surface (Sugioka *et al.* 2000). Of course, the most important characteristic that directly related some of these events to magmatic activity was their occurrence prior to large volcanic eruptions (e.g. Oura *et al.* 1992; Takeo 1992; Zobin & Levina 1998). Zobin (2001) interprets such large volcanic earthquakes as being the result of asperity failure due to high fluid pressure, leading to the opening of cracks that would eventually function as magma-transporting conduits during an eruption.

In other cases, however, this relationship between individual large events and volcanic activity is less clear, allowing different interpretations to be given in order to explain their occurrence. The 1980 Mammoth Lakes earthquakes in California can be considered as a typical example of such a case. Even though all three large ($M_L > 6$) events occurred near Long Valley caldera at 7–10 km depth, no volcanic activity that could be linked to these events was subsequently observed. The focal mechanisms obtained by inverting teleseismic waveforms showed a strong deviation from the double-couple model, leading Julian & Sipkin (1985) and Sipkin (1986) to conclude that the events may have been caused by opening of tensile cracks under high fluid pressure. On the other hand, Wallace (1985) pointed out that an equally realistic explanation for the large non-double-couple components is that of faulting complexity, suggesting that each of these events may be composed of smaller (double-couple) subevents. Furthermore, it was shown that the spectra of these earthquakes were not in any respect different from the spectra of common tectonic events, casting doubt on their volcanic nature (Priestly *et al.* 1985).

Ekström (1994) searched the Harvard CMT catalogue in order to find events with shallow hypocentral depths (<50 km), nearly vertical $T$-axis and large non-double-couple components that may be associated with volcanic processes. The search resulted in 18 events being found that fulfilled these criteria: eight of them were randomly distributed in seismic regions around the world, while the other ten were clustered around Bárdarbunga volcano in central Iceland. Bárdarbunga lies underneath the Vatnajökull glacier (Fig. 1) and along with the nearby Grimsvötn volcano, have been the centres of intense volcanic activity during historical times. The earthquakes occurred within a period of 18 years (1976–1994), had moment magnitudes in the range of 5.1–5.6 and hypocentral depths of 3.3–6.7 km, while the percentage of their non-douple-couple component was in the range of 48–82 per cent. However, none of these earthquakes was associated with any kind of volcanic activity, leaving both fluid injection and faulting complexity as equally good explanations for their anomalous nature.

In contrast, on 1996 September 29 a similar large earthquake occurred in Bárdarbunga followed 2 days later by an eruption that took place in the area between Bárdarbunga and Grimsvötn. In this paper we take advantage of the available high-quality broad-band regional waveform data of this latter Bárdarbunga earthquake in an effort to investigate whether a magma injection source is consistent with the observations. First, we begin with a summary of previous studies regarding this particular earthquake and the subsequent volcanic eruption. Then we proceed to a description of the available data and a study of the waveforms in the time and frequency domains. The deviatoric and full moment tensors for this event are determined using a waveform inversion method suitable for regional data. Finally, we discuss our results in the context of the magma injection hypothesis and suggest a possible physical mechanism that may explain the observations.

## 2 PREVIOUS SEISMOLOGICAL STUDIES

Teleseismic data of the Bárdarbunga event were inverted in order to recover its focal mechanism, depth and rupture history using two different methods: (1) Nettles & Ekström (1998) used a modified version of the Harvard CMT algorithm, which fits first arriving surface waves at periods of 40–150 s. The synthetic seismograms were calculated using ray theory and included reflections and conversions near the source; (2) Zobin (1999) used a finite fault parametrization method (Hartzel & Heaton 1983) by choosing a fault plane of fixed dimensions and orientation, embedded at an appropriate depth in the crustal structure of the source region. The fault plane was chosen to be a $10 \times 10$ km$^2$ rectangle divided into 100 subfaults of $1 \times 1$ km$^2$ surface area.

The results obtained by the first method indicated the presence of a large CLVD component and the degree of deviation from the

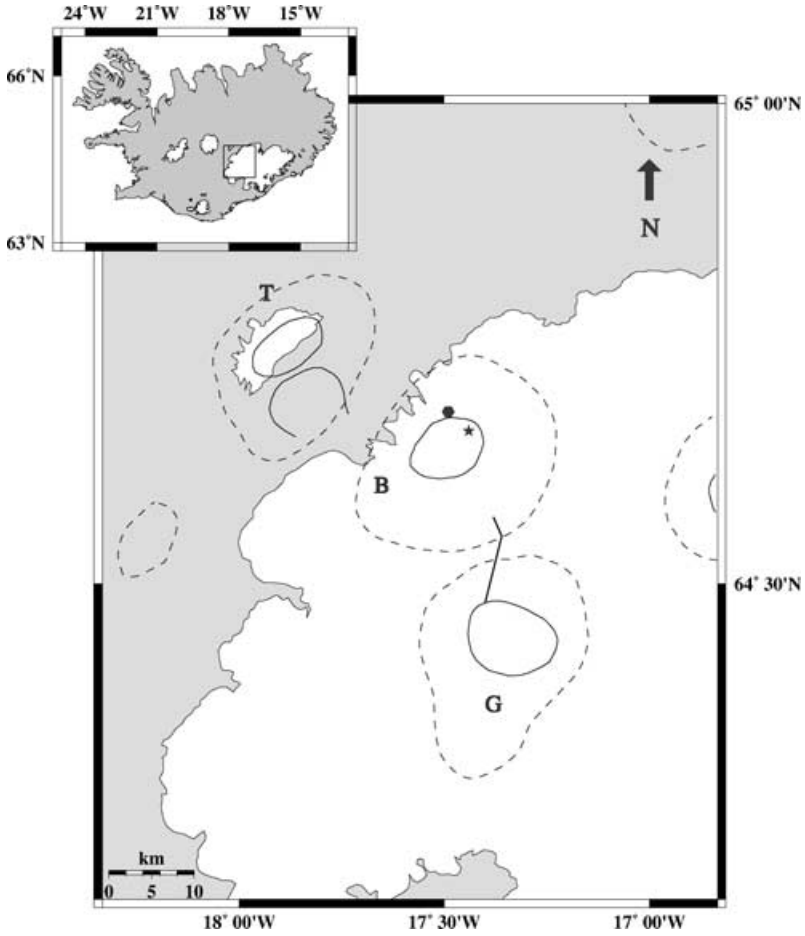


**Figure 1.** Map showing the NW part of the Vatnajökull glacier (unshaded terrain is ice covered: T, Tungafellsjökull; B, Bárdarbunga; G, Grimsvötn). Solid curves represent the outline of calderas, dashed curves the outline of central volcanoes. The epicentre of the Bárdarbunga earthquake located by Konstantinou *et al.* (2000) is shown by a star, while the epicentre located by the Icelandic Meteorological Office is shown by a hexagon. The thick line between the two volcanoes indicates the fissure observed during the 1996 eruption that followed the earthquake. The inset shows the relative location of NW Vatnajökull on the map of Iceland.

douple-couple mechanism was estimated using the dimensionless parameter $\epsilon$:

$$\epsilon = \frac{-\lambda_2}{\max(|\lambda_1|, |\lambda_3|)}, \quad (1)$$

where $\lambda_1$, $\lambda_2$ and $\lambda_3$ are the diagonal elements of the moment tensor in the principal axis coordinate system, ordered such that $\lambda_1 \geq \lambda_2 \geq \lambda_3$. For the Bárdarbunga event $\epsilon = 0.3$, whereas an $\epsilon$ value of zero corresponds to a pure douple-couple and a value of $\pm 0.5$ to a pure CLVD. The optimum depth for a point source was found in the range 3–7 km, with a value of 3.6 km yielding the best fit between observed and synthetic waveforms. The duration of the source time function was 5 s, while the scalar moment magnitude was estimated as 5.6.

Nettles & Ekström (1998) interpreted the large non-douple-couple component as being the result of a complex faulting process rather than a magma injection event based on the following arguments: (1) no volcanic activity was observed near the epicentre of this event; (2) magma injection in the form of a dyke or sill may not cause events of such large magnitude; (3) the epicentres of the aftershocks that followed delineated the rim of the Bárdarbunga caldera that could imply rupture along a curved plane. Nettles & Ekström (1998) further suggested that this event may have been caused by thrust motion on planes of varying strike that form an outward-dipping cone-shaped ring-fault beneath the Bárdarbunga caldera.

The second method also indicated a complicated rupture history, which was interpreted as the breaking of an asperity beneath Bárdarbunga due to an inflating magma chamber. The optimum hypocentral depth was found to be 4 km and the final slip on the fault was represented by an ellipse-shaped rupture having a maximum displacement of 45 cm. The broken asperity was found to extend from 3 to 6 km depth, thus having a vertical length of 3 km.

The Bárdarbunga event was followed by a swarm of low-frequency (1–2 Hz) events with epicentres that delineated the caldera rim. In the afternoon of the same day the seismic activity started to decline, but resumed again during the evening with a swarm of mixed frequency events (1–4 Hz) migrating towards Grimsvötn. During the next 2 days (September 30–October 1) the onset of the subglacial eruption took place, while mixed-frequency events occurred in the area between the two volcanoes. The eruption became subaerial on the afternoon of October 2 when a fissure was formed and over the days that followed the seismic activity started to decline. Volcanic tremor was detected prior to the eruption as a low-amplitude signal around five narrow frequency bands (0.5–0.7, 1.6, 2.2, 2.8, 3.2 Hz) changing its frequency content to broad-band after the onset of the subglacial eruption in October 1. The locations and classification of

the seismic signals along with a study of the co-eruptive tremor can be found in Konstantinou *et al.* (2000) and Konstantinou (2002).

## 3 DATA COLLECTION AND CHARACTERISTICS

At the time of the occurrence of the Bárdarbunga event a temporary (HOTSPOT) and one permanent (SIL) network were operational in Iceland (Fig. 2). HOTSPOT (Allen *et al.* 1999) was a joint project between Princeton and Durham Universities, the Icelandic Meteorological Office and the US Geological Survey, having as its primary purpose the collection of high-quality digital data of teleseismic and local events. HOTSPOT consisted of 30 broad-band three-component seismometers recording continuously at a rate of 20 samples $s^{-1}$, while absolute timing was provided by GPS receivers. The South Iceland Lowlands (SIL) network is operated by the Icelandic Meteorological Office and consisted (at the time of the eruption) of 30 stations with broad-band or short-period sensors, recording local earthquake data using a triggering mechanism at a rate of 100 samples $s^{-1}$.

In this study we have only used data recorded by HOTSPOT and Table 2 gives a list of the stations that were operational at the time of the earthquake. The epicentre for this event was located inside the Bárdarbunga caldera (64.66°N, −17.44°E) at a depth of 7 km. This location was determined after a damped iterative inversion of *P*-wave first arrivals (Konstantinou *et al.* 2000) using an unpublished 1-D crustal model (Table 3), which is used for routine earthquake locations by the Icelandic Meteorological Office. At this point it should be noted that the location obtained by the Icelandic Meteorological Office using only SIL arrival times (64.68°N, −17.49°E, 4.04 km) is approximately 5 km away from the HOTSPOT location, thus the epicentre lies outside the caldera (see Fig. 1). This difference may probably be attributed to two reasons: (1) the station geometry of the SIL network covers azimuths only in the NE and SW directions with respect to the source and (2) as will be discussed shortly afterwards, the first arrivals of this event are quite emergent,

**Table 2.** List of HOTSPOT stations that were operational at the time of the Bárdarbunga event.

| Station | Lat. (°N) | Long. (°E) | Elev. (m) | Sensor type |
|---|---|---|---|---|
| HOT01 | 64.494 11 | −21.167 89 | 205.0 | CMG-3ESP |
| HOT02 | 64.745 82 | −22.232 26 | 40.0 | CMG-3ESP |
| HOT03 | 64.907 60 | −23.852 70 | 35.0 | CMG-40T |
| HOT04 | 65.180 47 | −22.423 12 | 40.0 | CMG-3ESP |
| HOT05 | 65.109 69 | −21.096 37 | 35.0 | CMG-3ESP |
| HOT06 | 65.705 02 | −21.677 87 | 25.0 | CMG-3ESP |
| HOT07 | 65.598 39 | −22.509 99 | 40.0 | CMG-3ESP |
| HOT08 | 65.609 82 | −24.161 41 | 8.0 | CMG-3ESP |
| HOT09 | 65.873 88 | −23.486 61 | 50.0 | CMG-3ESP |
| HOT10 | 65.926 69 | −22.428 22 | 7.0 | CMG-3ESP |
| HOT12 | 65.670 71 | −19.599 65 | 38.0 | CMG-3T |
| HOT13 | 65.686 00 | −18.099 91 | 24.0 | CMG-3T |
| HOT14 | 65.302 80 | −18.256 50 | 245.0 | CMG-3ESP |
| HOT15 | 66.121 00 | −15.172 00 | 20.0 | CMG-3ESP |
| HOT16 | 65.540 90 | −13.753 50 | 5.0 | CMG-3ESP |
| HOT17 | 65.255 00 | −14.504 00 | 80.0 | CMG-3ESP |
| HOT18 | 65.166 00 | −15.308 70 | 342.0 | CMG-3ESP |
| HOT19 | 64.812 00 | −14.100 00 | 50.0 | CMG-3ESP |
| HOT21 | 63.876 84 | −16.640 62 | 20.0 | CMG-3ESP |
| HOT22 | 63.769 84 | −18.130 68 | 65.0 | CMG-3ESP |
| HOT23 | 64.406 70 | −17.266 30 | 1730.0 | CMG-3ESP |
| HOT24 | 64.886 30 | −15.353 70 | 600.0 | CMG-3ESP |
| HOT25 | 65.054 00 | −16.652 00 | 920.0 | CMG-40T |
| HOT27 | 65.200 00 | −19.590 00 | 450.0 | CMG-3ESP |
| HOT29 | 65.728 00 | −14.838 00 | 60.0 | CMG-40T |

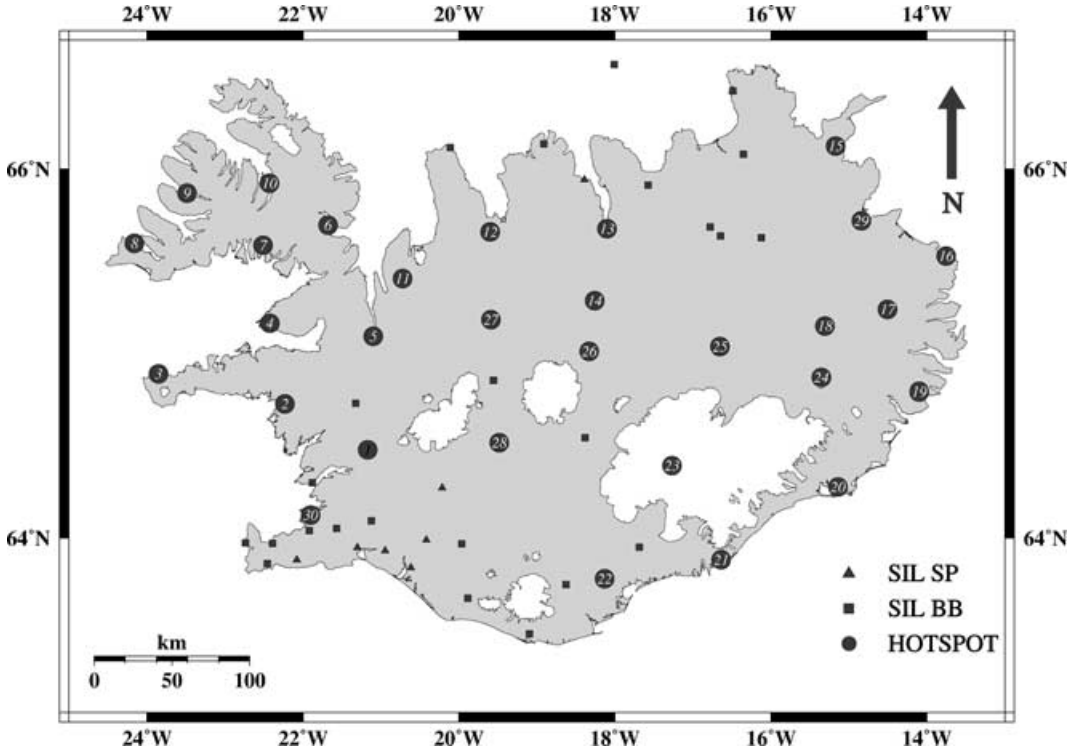


**Figure 2.** Map showing the locations of temporary (HOTSPOT) and permanent (SIL) seismic networks that were operational at the time of the Bárdarbunga earthquake (SP, short-period stations; BB, broad-band stations).

**Table 3.** Crustal model used to locate events.

| Layer thickness (km) | *P*-wave velocity (km s$^{-1}$) |
|---|---|
| 1.00 | 3.53 |
| 2.00 | 4.47 |
| 3.00 | 5.16 |
| 4.00 | 5.60 |
| 6.00 | 5.96 |
| 9.00 | 6.50 |
| 20.00 | 6.73 |
| 32.00 | 7.20 |
| 90.00 | 7.40 |

introducing errors in the phase picking at the more distant SIL stations where the signal-to-noise ratio is expected to be lower.

The velocity waveforms of the Bárdarbunga event show an emergent onset characterized by a low-amplitude but high-frequency signal that is superposed on a longer-period waveform (Fig. 3). The polarity of the first motion indicates a compressional *P* wave for some of the stations, while in others it is difficult to determine it. However, at all stations this emergent low-amplitude onset is followed by a clear dilatation that in some cases can be mistaken as the first motion on the seismogram. In the frequency domain, the spectra exhibit little energy present above 1 Hz and a pronounced peak around the corner frequency between 0.15 and 0.26 Hz (Fig. 4). In addition, several other peaks at frequencies higher than 0.3 Hz are common among stations azimuthally distributed around the source, precluding the possibility that they may be the result of path or site effects. Based on waveform appearance (emergent onsets, lack of clear *S* phases) and frequency content this event may be characterized as a low-frequency earthquake following the classification scheme for volcanoseismic signals suggested by McNutt (1996).

## 4 MOMENT TENSOR INVERSION

### 4.1 Data preparation and method

The preparation of the data for the moment tensor inversion involved first of all a quality check of the three-component waveforms.

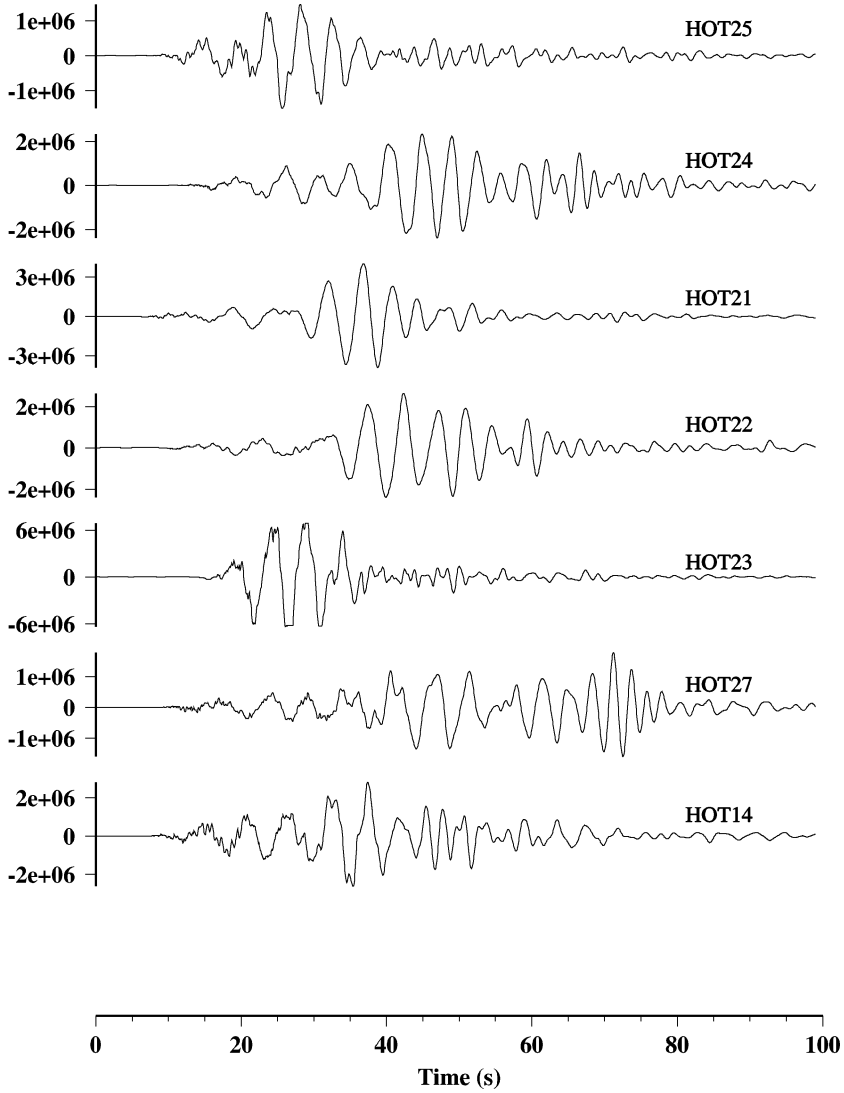


**Figure 3.** Vertical component velocity waveforms of the Bárdarbunga earthquake recorded at the closest (<150 km) HOTSPOT stations. The seismograms are arranged in order of increasing azimuth around the source (amplitudes in arbitrary units). Note the emergent onset and low-frequency content apparent at all stations around the source.

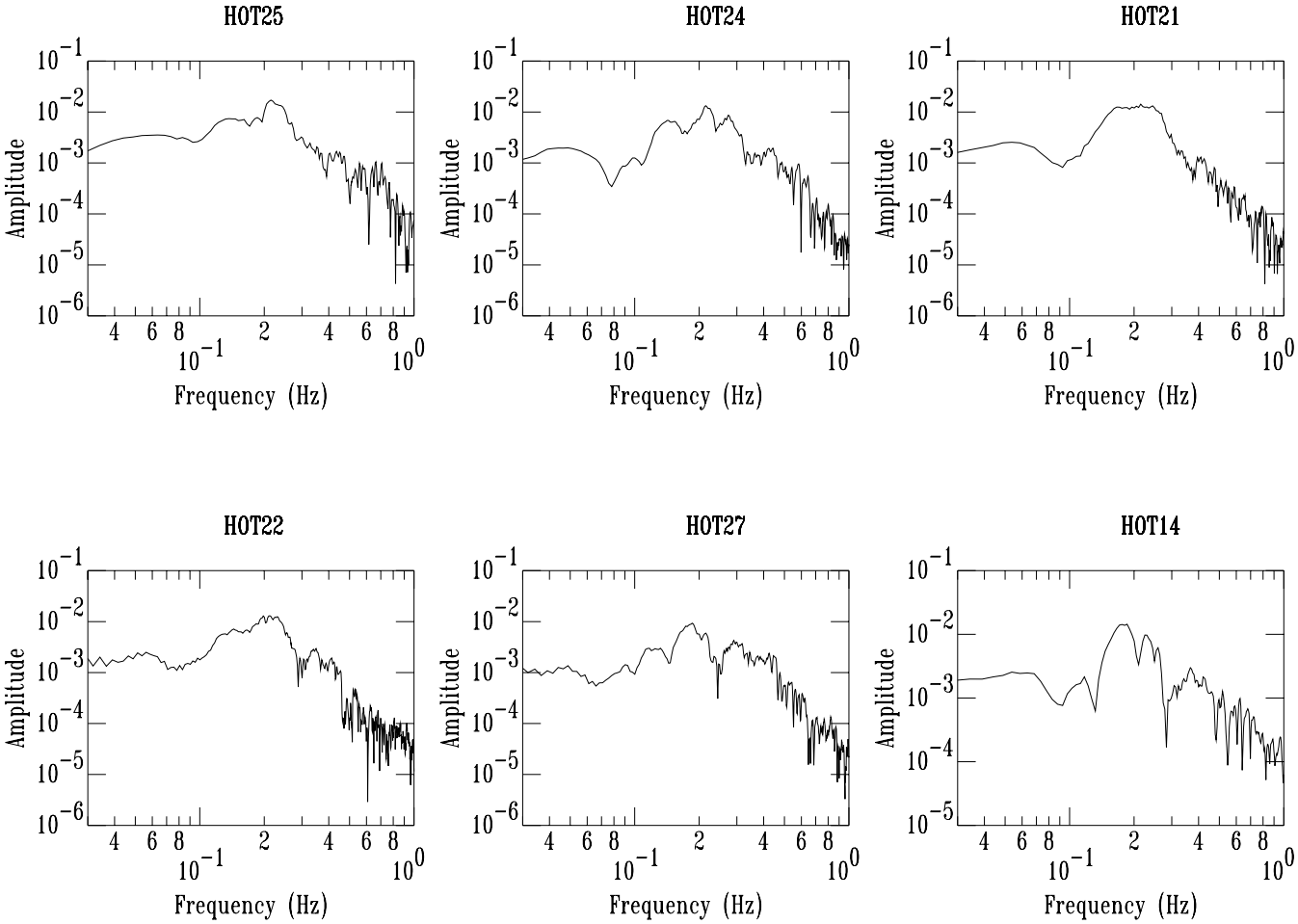


**Figure 4.** Vertical component amplitude spectra obtained from the waveforms shown in the previous figure after removing the instrument response (amplitude units in cm).

After this check the data from station HOT23 were excluded since the recorded signal was clipped. Also, a number of horizontal components (mostly from stations near the coast) had to be excluded because they were contaminated with long-period noise. The instrument response was then removed from the rest of the data and the horizontal seismograms were rotated into the radial-transverse coordinate system with respect to the location obtained using HOTSPOT arrival times. Finally, the data were bandpass filtered between 0.01–0.05 Hz forwards and backwards (in order to eliminate any phase distortion) using a two-pole Butterworth filter. The choice of this particular bandwidth for inverting the data stems from the fact that 20–100 s period waves are relatively insensitive to lateral heterogeneity and finer-scale velocity structure of which we have no detailed knowledge.

Green's functions were calculated using the reflection-matrix method of Kennett (1983) as implemented by Randall (1994). The velocity model used for the calculation is the same as has been used for the earthquake locations (Table 2) and is a 1-D average of the tomographic model for Iceland published by Bjarnasson *et al.* (1993). Once computed, the Green's functions were bandpass filtered between 0.01 and 0.05 Hz in the same way as the data.

The waveforms were modelled using a time-domain linear moment tensor inversion with a point-source approximation. The moment tensor elements are estimated by minimizing the least-squares misfit between the observed and predicted waveforms. This is achieved by solving a system of linear equations that is represented in matrix notation as $\mathbf{d} = \mathbf{Gm}$, where $\mathbf{d}$ is the vector that contains the observed three-component displacements from each station, $\mathbf{G}$ is the matrix with columns that are the Green's functions and $\mathbf{m}$ is a vector containing the moment tensor elements. Details of the algorithm can be found in Langston *et al.* (1982).

### 4.2 Inversion results

We first inverted the data, imposing the condition of a vanishing isotropic component ($M_{xx} + M_{yy} + M_{zz} = 0$) and assuming a step source time function. The inversions were repeated for depths in the range of 0.5–16 km at a constant step of 1.5 km. Initially no weighting was applied to the data so that more importance is given during the inversion to the stations closer to the source. The inversions were subsequently repeated for the same range of depths after weighting the data according to their distance from the source. Examples of the inversion results for particular stations are shown in Fig. 5. The average fractional misfit versus depth curves for the two inversions sets (Fig. 6) are very close at 0.5–3.5 km and 14 km depths, while they are almost identical everywhere else; more importantly both curves exhibit a clear minimum at a depth of 3.5 km. The CLVD percentage for the unweighted and weighted inversion at that depth was estimated as $2\epsilon \times 100$ per cent (where $\epsilon$ is given by equation 1) and was found to be 60.4 and 60.8 per cent, respectively. The best

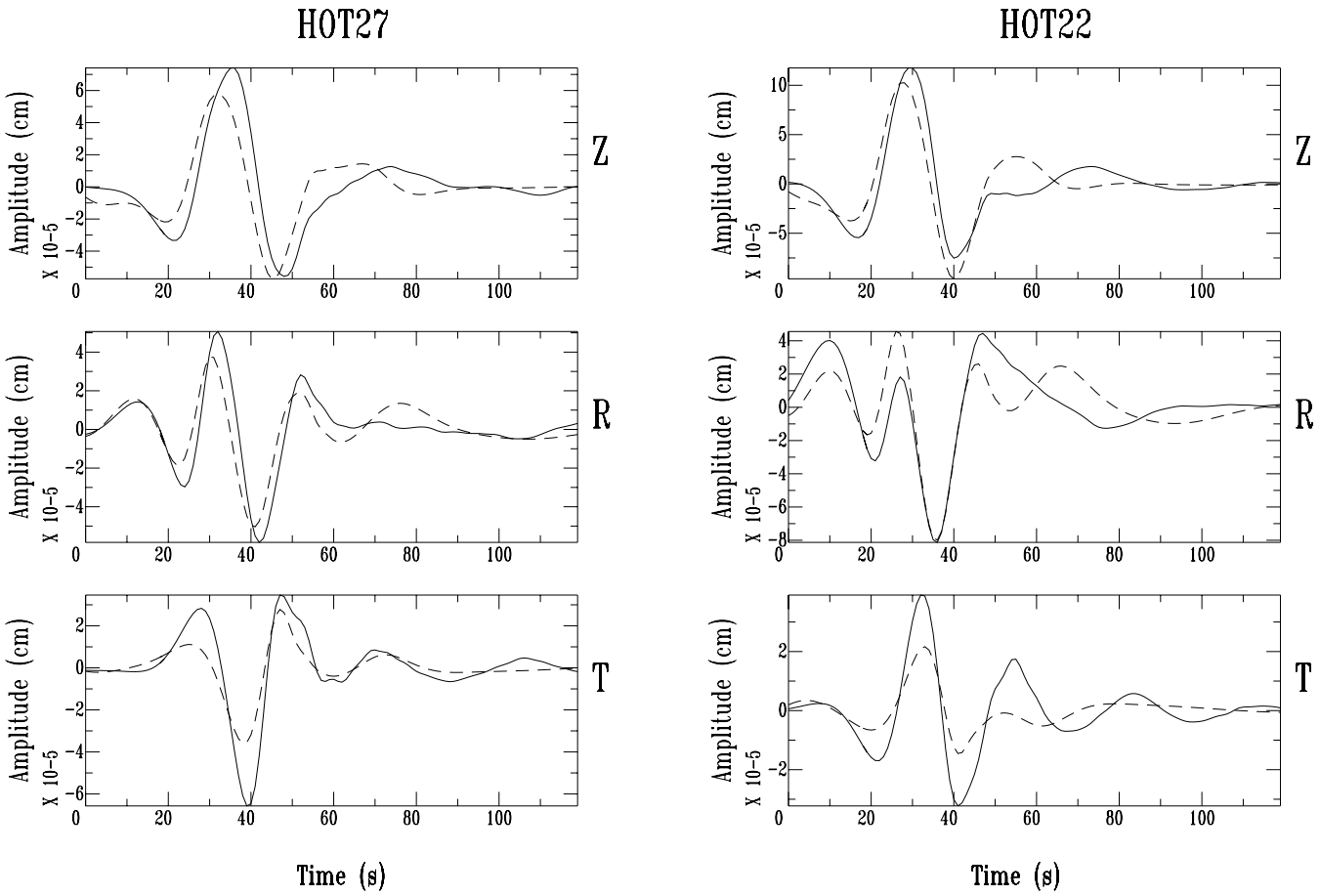


**Figure 5.** Results of the inversion for the deviatoric moment tensor at 3.5 km depth for two HOTSPOT stations without applying distance-dependent weighting. Solid lines represent the observed data and dashed lines the synthetics (Z, vertical; R, radial; T, transverse).

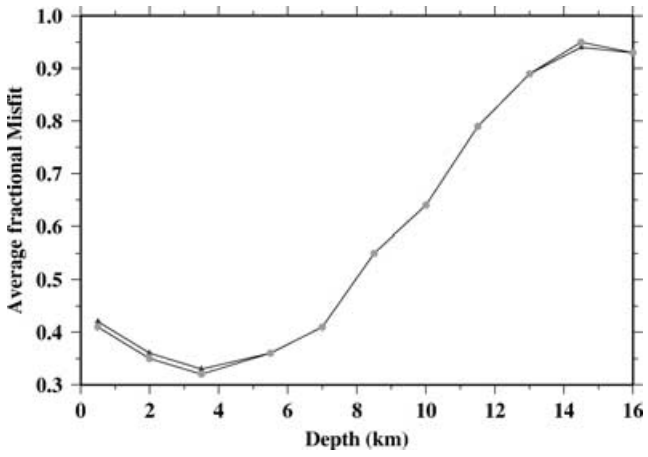


**Figure 6.** Average fractional misfit-versus-depth curves resulting from the inversions of all the available HOTSPOT data. Black triangles indicate the misfits when the inversions were performed without distance-dependent weighting of the data. Grey circles indicate the misfits when the inversions were performed with distance-dependent weighting.

double-couple solutions in both cases are very similar, indicating pure thrust motion, while the moment magnitude for both was estimated as 5.4 in good agreement with the Harvard CMT solution.

The next step was to take into account the possibility of a non-zero isotropic component and invert the data for the best-fitting full moment tensor at 3.5 km depth. The results of this inversion showed a reduced CLVD component of 47.2 and an 8.5 per cent implosive isotropic component, the percentage of which was estimated as $k \times 100$ per cent, where $k$ is given by

$$k = \frac{M^{\mathrm{iso}}}{M^{\mathrm{iso}} + M^{\mathrm{dev}}} \tag{2}$$

where $M^{\mathrm{iso}}$ is the isotropic and $M^{\mathrm{dev}}$ is the deviatoric scalar moment. Another interesting result of the full moment tensor inversion is that the sense of motion in the best double-couple solution changed from thrust to normal faulting while maintaining the same orientation of fault/auxiliary planes with the deviatoric moment tensor solution. Fig. 7 shows a comparison of the distribution of the fractional misfits obtained after the deviatoric and full moment tensor inversions for a depth of 3.5 km at all stations.

In an effort to check whether our rather simplistic choice of a source time function may have biased our inversion results, we repeated the procedure outlined above using the source time function derived for this event by Nettles & Ekström (1998). This source time function could be approximated by a triangle with a rise and fall time of 3 and 2 s, respectively. The inversion results (using weighted and unweighted data) for the deviatoric and full moment tensor showed no significant difference from the results obtained assuming a step source time function.

The results of all the inversions we performed are summarized in Fig. 8. It can be seen that the misfit for the full moment tensor

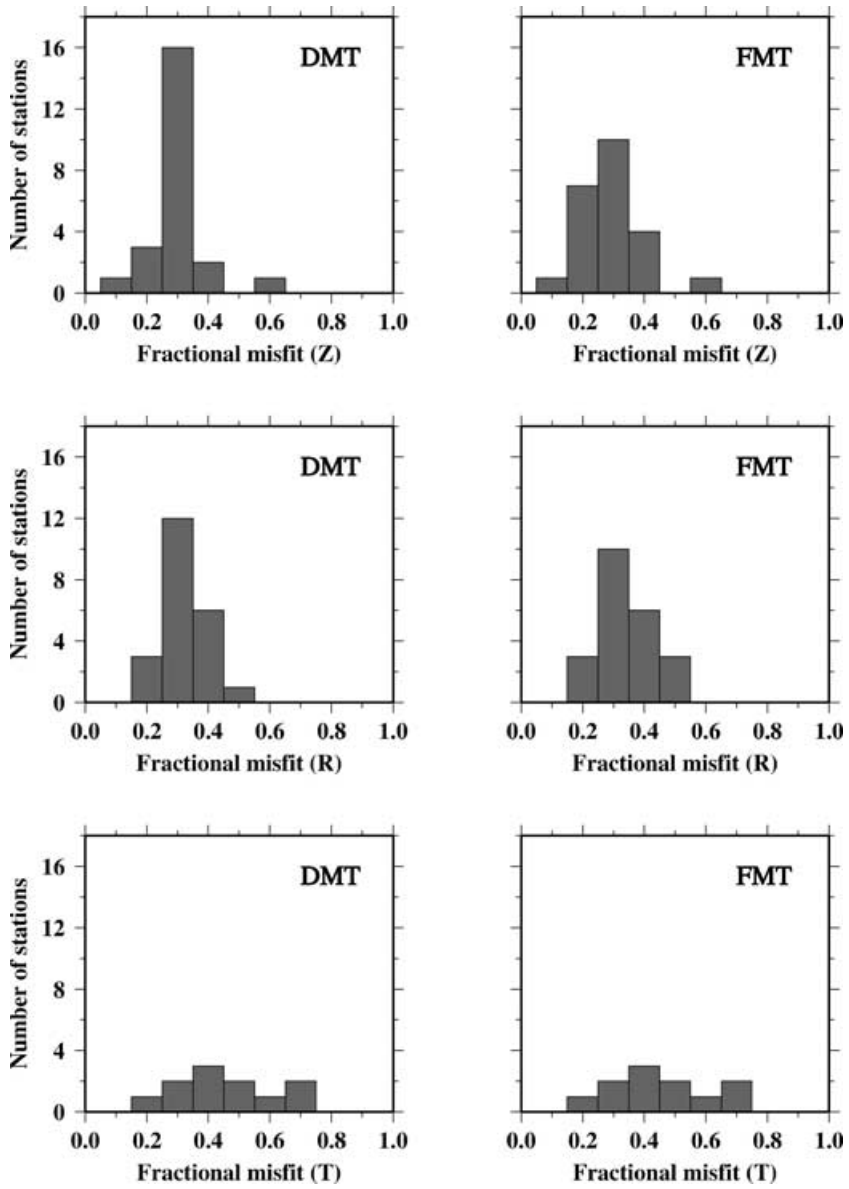


**Figure 7.** Histograms showing the distribution of the fractional misfits for each component (Z, vertical; R, radial; T, transverse) at all HOTSPOT stations for the inversion at 3.5 km depth (DMT, deviatoric moment tensor; FMT, full moment tensor) without distance-dependent weighting. The small number of transverse components is a result of many of them being excluded from the inversion because of contamination with long-period noise.

solution is only slightly lower than the misfits for the deviatoric solutions. In theory, a model that has a greater number of unknowns (such as the full moment tensor compared with the deviatoric) is expected to fit the data better. However, a statistical F-test should be used in order to determine whether a model with a change in the number of free parameters fits the data *significantly* better than might be expected from random fluctuations (Menke 1989). The F-test is based on the null hypothesis that the variances of two samples are the same and the F statistic is defined as the ratio of the two data variance estimates. Critical values of F above which the difference in the variance is significant can be calculated from the F distribution (see Press *et al.* 1992, for details). The F-test for our data indicated that the null hypothesis cannot be rejected but with a confidence level of not more than 76 per cent. The inability of the F-test to reject the full moment tensor solution at an acceptable confidence level leaves open the possibility of a non-zero isotropic component for the Bárdarbunga event.

## 5 DISCUSSION

### 5.1 The magma injection hypothesis

An alternative explanation for the strongly non-double-couple mechanism of the 1996 September 29 Bárdarbunga event is that of magma/fluid injection. However, in order to be able to decide on the validity of such an interpretation, the data should be consistent with results of theoretical modelling of such a process. The dynamics of an expanding fluid-filled crack formed after the failure of a barrier have been studied in 2-D and 3-D by Chouet & Julian (1985) and Chouet (1986), respectively. Under some simplifying assumptions

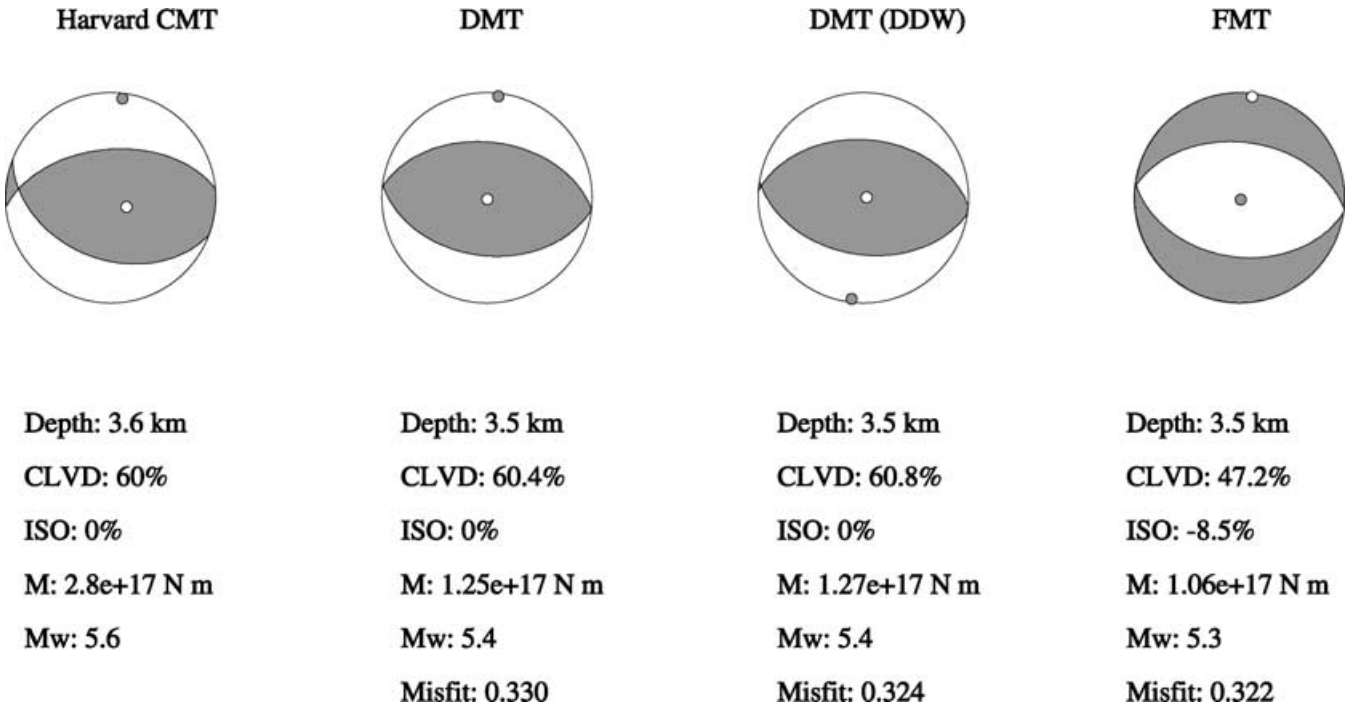


**Figure 8.** Summary of the inversion results obtained in this study for the deviatoric moment tensor (DMT), deviatoric moment tensor with distance-dependent weighting (DDW) and full moment tensor (FMT) as compared with the Harvard CMT solution of Nettles & Ekström (1998). The beachballs represent the best double-couple solutions determined by the inversions, plotted in an equal area lower hemisphere projection. Grey areas indicate compressions and white areas dilatations. *P* axes are plotted as grey circles and *T* axes as white circles.

concerning the nature of the fluid (incompressible, low viscosity, able to sustain acoustic waves), the crack (rectangular geometry, elastic walls) and the flow regime inside the crack (laminar flow), this modelling indicated that events generated by such a process should exhibit the following characteristics.

(1) The first motion on the seismograms at all azimuths is a low-amplitude and high-frequency compressional signal that indicates the barrier failure and the opening of the crack. This signal is superimposed on a longer-period dilatation that is the result of a partial closing due to decreasing pressure in the fluid once it has been injected into the crack. In terms of an equivalent force system this means that an implosive isotropic component should be superimposed to a CLVD (Haskell 1964; Julian *et al.* 1998).

(2) The spectrum of an event generated by fluid injection contains a series of sharp peaks that represent the lateral and longitudinal oscillation modes of the crack.

Even though the polarity of the first motion at some stations is subject to uncertainty, the waveform characteristics and moment tensor inversion results presented earlier in this study are consistent with an interpretation involving magma injection for the Bárdarbunga earthquake. Another indication that favours such an interpretation stems from the comparison of the spectra shown in Fig. 4 with those calculated for the seismic radiation of a tensile crack by Walter & Brune (1993). In the case of an opening and closing elliptical crack the authors found that the azimuthally averaged spectrum would have reduced lower frequencies leading to a peak near the corner frequency. This feature was quite prominent in the spectra of the Bárdarbunga event at all stations and is in agreement with an overall volume decrease at the source indicated by the small implosive isotropic component. It should be noted that we compare directly the observed and theoretical spectra, without performing any corrections for propagation effects, for the following reasons: (1) our comparison refers to the spectral shape around the corner frequency (0.25 Hz) and *lower* frequencies that are expected to be much less influenced by propagation effects; (2) Walter & Brune (1993) note that different fall-offs for the higher frequencies have only a slight effect on the spectral shape below the corner frequency in their model; and (3) existing crustal models for Iceland are not so accurate as to be able to resolve the velocity structure details in the upper crust, necessary for such corrections.

### 5.2 Estimation of geometrical and physical parameters

Assuming that the crack generated by the fluid injection has approximately a rectangular shape, then its horizontal length should be about 10 km based on the distribution of the aftershocks that followed the Bárdarbunga event (Konstantinou *et al.* 2000). The vertical length can be inferred from the study of the mainshock rupture by Zobin (1999) that reports a vertical rupture length of 3 km. These numbers imply a rupture area of 30 km$^2$ and in order to check further whether this is consistent with an $M_w = 5.4$ event we use an empirical relationship that gives the rupture area $A$ as a function of moment magnitude (Wells & Coppersmith 1994)

$$\log A = -3.49 + 0.91 M_w. \quad (3)$$

This relationship was obtained after linear, least-squares regression of 148 earthquakes and is valid for moment magnitudes in the range 4.8–7.9. We calculate an expected rupture area for the Bárdarbunga event of 26.54 km$^2$ that is quite close to our initial estimate considering the uncertainties involved in the estimation of the crack dimensions.

The volume $V$ of the fluid injected into the newly formed crack is proportional to the scalar moment of the resulting earthquake and if

the crack is assumed to be rectangular, Müller (2001) suggests the use of the following equation for volume estimations:

$$V = \frac{M}{\lambda + 2\mu/3}, \tag{4}$$

where $M$ is the scalar moment and $\lambda$, $\mu$ are the Lamé constants. Assuming that $\lambda = \mu$ and taking into account that the rigidity modulus in volcanic areas is much less than that expected in non-volcanic areas we take $\mu = 0.5 \times 10^{10}$ N m$^{-2}$ as suggested by Smith *et al.* (1996). Using as scalar moment the value derived from the deviatoric moment tensor inversion ($1.25 \times 10^{17}$ N m), we obtained a volume of $15 \times 10^6$ m$^3$ of injected fluid. This value along with the crack dimensions inferred previously suggest a crack opening of 0.5 m, which represents a reasonable value based on thickness measurements of exhumed dykes in Iceland (Gudmundsson 1995).

The viscosity is perhaps the only property of the injected fluid that we can directly calculate and is given by the equation (Julian & Sipkin 1985)

$$\eta = \frac{\tau \Delta P}{12\gamma^2}, \tag{5}$$

where $\eta$ is the viscosity, $\tau$ is the source duration of the earthquake, $\Delta P$ is the pressure difference driving the fluid in the crack and $\gamma$ is the aspect ratio of the crack (vertical length divided by thickness). A value of $\tau = 5$ s is taken based on the duration of the source time function reported by Nettles & Ekström (1998), while an aspect ratio of 6000 is calculated for our crack dimensions. The pressure difference $\Delta P$ is usually comparable in magnitude to the strength of the rock, which for Iceland an average value has been determined by *in situ* measurements to be $3.5 \times 10^6$ Pa (Haimson & Rummel 1982). Using these values we obtain a fluid viscosity of 0.04 Pa s, which precludes the possibility that the injected fluid may be magma, if our aspect ratio and crack dimension estimates are correct. This result is similar to those found by other investigators (Julian & Sipkin 1985; Kanamori *et al.* 1993; Dreger *et al.* 2000), which concluded that such seismic events are usually too short to be explained by the injection of low-viscosity magma and that other pressurized fluids (exsolved volatiles or supercritical water heated by magma) are more probable alternatives. Finally, the flow rate of the fluid in the crack will be equal to $V/\tau$, which yields a value of $3 \times 10^6$ m$^3$ s$^{-1}$.

### 5.3 Possible physical mechanisms of fluid injection

Current volcanological models based on studies of exhumed volcanic systems suggest that most Icelandic central volcanoes consist of a shallow (2–6 km) magma chamber filled with partially molten material, which is fed by a deeper (8–12 km) reservoir through a swarm of subvertical dykes (Gudmundsson 1995). Even though very little is known concerning the structure of the volcanic systems underneath the Vatnajökull glacier, the depth of the shallow magma chamber and its position relative to the broken asperity are important parameters in our interpretation effort. Therefore, in the context of the fluid injection hypothesis we will consider two possible scenarios.

(a) *The magma chamber is situated below (∼6 km) the asperity.* This situation implies the failure of the roof of the magma chamber and the injection of pressurized fluid into the crack. Indeed, Parfitt *et al.* (1993) recognized that a layer of $CO_2$ or foam near the roof of a basaltic magma chamber is the most likely cause for the generation of a fracture (and a subsequent summit eruption) and the case of injected magma volatiles is in agreement with our previous results. However, even though we cannot completely rule out this model, we consider it as less likely for the following reasons: (1) Parfitt *et al.* (1993) noted that the gas layer should be tens to hundreds of metres thick (depending on the radius of the chamber) in order for the roof to fail. In terms of magma composition this means that the total content of $CO_2$ should be at least 0.3 wt per cent for such a layer to form, a value that is the maximum possible for basaltic magmas; (2) the locations of the aftershocks shifted systematically southwards and the volcanic activity was observed 20 km away from the epicentre of the Bárdarbunga event, suggesting a lateral rather than a summit intrusion (Einarsson *et al.* 1997; Konstantinou *et al.* 2000); (3) studies of the crustal structure of other central volcanoes in Iceland (Gudmundsson *et al.* 1994) combined with the thinning of the upper crust in NW Vatnajökull (Darbyshire *et al.* 1998) point to the possibility of a depth for the Bárdarbunga magma chamber shallower than 6 km.

(b) *The magma chamber is situated above (∼ 3 km) the asperity.* This case can be realized if one of the dykes extending from the deeper reservoir reaches the asperity and the flow of magma in the dyke is stopped (Fig. 9). Since the upper crust in the Vatnajökull area is expected to be water-saturated due to the presence of the glacier, it is possible that this water was heated by the magma and as a result its specific volume may have increased up to 30 times (Kanamori *et al.* 1993). The pressure build-up may then have resulted in the asperity failure. One criticism against such a model would be that the rock near the magma chamber (depths 3–4 km) would be too hot to sustain a crack. However, Gudmundsson (1988) concludes that this may not be necessarily so based on the following arguments: (1) in order for the rock surrounding the magma chamber to exhibit ductile behaviour, its temperature should exceed 700 °C, but this is unlikely in areas where water can percolate the host rock thus keeping the temperature below this threshold; (2) the occurrence of a large number of dykes and inclined sheets near to extinct shallow magma chambers in Iceland and elsewhere, indicates that near to such chambers the crustal rock is able to sustain stress differences

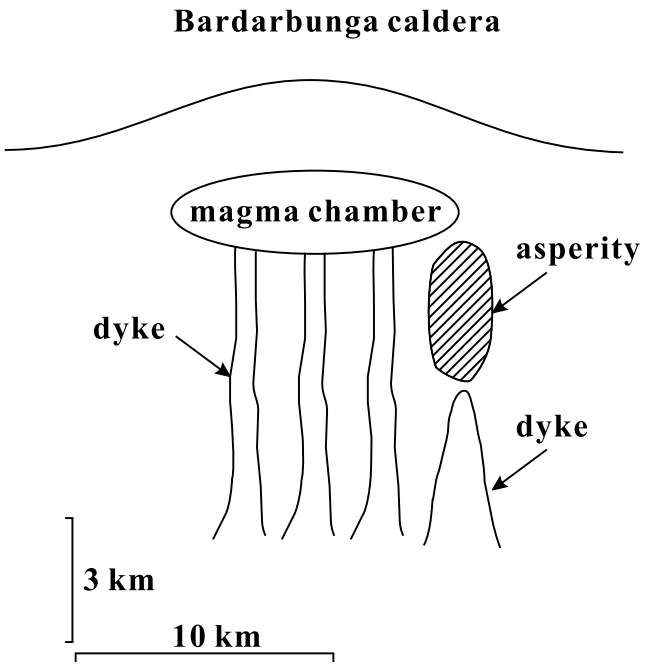


**Figure 9.** Cartoon illustrating the possible configuration underneath Bárdarbunga volcano, that may have caused the observed anomalous event (see the text for more details).

that are probably of the order of the tensile strength of the crust, otherwise such features would not form.

The latter interpretation is also more consistent with two other observations: (1) the spectral analysis indicated a sharp reduction in amplitude of volcanic tremor 3.5 h before the Bárdarbunga earthquake (Konstantinou *et al.* 2000), probably reflecting a sudden decrease of the flow of magma in the shallow magma chamber. This time may also be the time needed for heating the water and increasing the pressure to the required levels for rupturing the asperity; (2) a 23 min (1380 s) gap between the mainshock and the occurrence of the first aftershock was observed (Konstantinou 2001) and if we use this time as a source duration for eq. (5) we obtain a viscosity value for the fluid of 11.18 Pa s, which is at the lower end of possible viscosities for basaltic magmas (Philpotts 1990). Therefore, it is possible that once the asperity broke, magma flowed into the magma chamber through the newly formed crack increasing the pressure and changing the equilibrium conditions inside it. This would have the effect of increasing the stresses in the surrounding rocks and thus inducing seismicity. Eventually this would lead to a lateral emplacement of magma and a flank eruption as was subsequently observed.

Ultimately, it may be impossible to decipher unambiguously, based on existing data, whether the latest Bárdarbunga event (and possibly the others) was caused by the mechanism of fluid injection described above or complex faulting processes such as the failure of a ring-fault. The results of this study indicate, however, that the data are consistent with a magma-related source interpretation and such a mechanism should not be considered as less likely.

## 6 CONCLUSIONS

The main conclusions of this study can be summarized as follows.

(1) The seismograms from the 1996 September 29 earthquake at Bárdarbunga volcano are characterized by emergent waveforms, lack of clear *S* wave phases, low-frequency content ($<1$ Hz) and prominent spectral peaks at the corner frequency and at higher frequencies.

(2) A linear, time-domain moment tensor inversion of the available regional data was performed for the recovery of the deviatoric and full moment tensors. The results revealed a large CLVD percentage ($\sim$60 per cent) and a hypocentral depth of 3.5 km for the deviatoric solution in good agreement with the previously published Harvard CMT solution. The full moment tensor solution also revealed a 8.5 per cent implosive isotropic component, which could not be rejected at an acceptable confidence level after perfoming an F-test.

(3) The inversion results seemed to be insensitive to the particular choice of a source time function or to the optional distance-dependent weighting of the data.

(4) Based on existing models of expanding fluid-filled tensile cracks, volcanological observations in Iceland and calculations of some physical parameters the Bárdarbunga event may have resulted from the formation of a 10 km $\times$ 3 km $\times$ 0.5 m crack beneath a shallow magma chamber. Taking into account the water saturation of the upper crust in Vatnajökull due to the overlying glacier, the failure of the rock and the crack opening was caused by the increased pressure of water heated by injected magma. The crack established connection with the shallow magma chamber functioning as a transport conduit for magma. The fluids that moved inside the chamber changed its internal pressure and equilibrium conditions, causing the occurrence of small earthquakes around it and the emplacement of a lateral dyke, resulting eventually in the observed flank eruption.

## ACKNOWLEDGMENTS

The HOTSPOT project was funded by National Environmental and Research Council (NERC) grant nos GST/02/1238 and GR3/10727, NSF grant no EAR 9417918 and supported by the US Geological Survey. IRIS/PASSCAL offered technical support and assistance in running the network. The first author would like to thank Ragnar Stefánsson for useful discussions regarding the 1996 Vatnajökull eruption and the anomalous events that occurred previously in that area. The critical comments of an anonymous reviewer helped to improve the original manuscript substantially. This research was supported by the National Research Council of Taiwan and by the Institute of Earth Sciences, Academia Sinica through a postdoctoral research fellowship awarded to the first author.

## REFERENCES

Allen, R.M. *et al.*, 1999. The thin hot plume beneath Iceland, *Geophys. J. Int.* **137,** 51–63.

Bjarnasson, I.T., Menke, M., Flóvenz, O.G. & Caress, D., 1993. Tomographic image of the Mid-Atlantic plate boundary in southwestern Iceland, *J. geophys. Res.,* **98,** 6607–6622.

Chouet, B.A., 1986. Dynamics of a fluid-driven crack in three dimensions by the finite difference method, *J. geophys. Res.,* **91,** 13 967–13 992.

Chouet, B.A. & Julian, B.R., 1985. Dynamics of an expanding fluid-filled crack, *J. geophys. Res.,* **90,** 11 187–11 198.

Darbyshire, F.A., Bjarnasson, I.T., White, R.S. & Flóvenz, O.G., 1998. Crustal structure above the Iceland mantle plume imaged by the ICEMELT refraction profile, *Geophys. J. Int.* **135,** 1131–1149.

Dreger, D.S., Tkalcic, H. & Johnston, M., 2000. Dilational processes accompanying earthquakes in Long Valley Caldera, *Science,* **288,** 122–125.

Einarsson, P., Brandsdóttir, B., Gudmundsson, M.T. & Björnsson, H., 1997. Centre of the Iceland hotspot experiences volcanic unrest, *EOS, Trans. Am. geophys. Un.,* **78,** 374–375.

Ekström, G., 1994. Anomalous earthquakes on volcano ring-fault structures, *Earth planet. Sci. Lett.,* **128,** 707–712.

Gudmundsson, A., 1988. Effect of tensile stress concentration around magma chambers on intrusion and extrusion frequencies, *J. Volc. Geotherm. Res.,* **35,** 179–194.

Gudmundsson, A., 1995. Infrastructure and mechanics of volcanic systems in Iceland, *J. Volc. Geotherm. Res.,* **64,** 1–22.

Gudmundsson, O., Brandsdóttir, B., Menke, M. & Sigvaldasson, G.E., 1994. The crustal magma chamber of the Katla volcano in south Iceland revealed by 2D seismic undershooting, *Geophys. J. Int.* **119,** 277–296.

Ishimoto, M., 1932. Existence of a quadrupole source at the seismic focus according to the study of the distribution of initial movements of seismic shocks, *Bull. Earthquake Res. Inst. Univ. Tokyo,* **10,** 449.

Haimson, B.C. & Rummel, F., 1982. Hydrofracturing stress measurements in the Iceland research drilling project drill hole at Reydarfjördur, Iceland, *J. geophys. Res.,* **87,** 6631–6649.

Hartzel, S.H. & Heaton, T.H., 1983. Inversion of strong ground motion and teleseismic waveform data for the fault rupture history of the 1979 Imperial Valley, California, earthquake, *Bull. seism. Soc. Am.,* **73,** 1553–1583.

Haskell, N.A., 1964. Total energy and energy spectral density of elastic wave radiation from propagating faults, *Bull. seism. Soc. Am.,* **54,** 1811–1841.

Julian, B.R. & Sipkin, S.A., 1985. Earthquake processes in the Long Valley caldera, California, *J. geophys. Res.,* **90,** 11 155–11 169.

Julian, B.R., Miller, A.D. & Foulger, G.R., 1998. Non-double-couple earthquakes—1. Theory, *Rev. Geophys.,* **36,** 525–549.

Kanamori, H., Ekström, G., Dziewonski, A., Barker, J.S. & Sipkin, S.A., 1993. Seismic radiation by magma injection: an anomalous seismic event near Tori Shima, Japan, *J. geophys. Res.,* **98,** 6511–6522.

Kennett, B.N.L., 1983. *Seismic Wave Propagation in Stratified Media,* Cambridge University Press, Cambridge.

Knopoff, L. & Randall, M.J., 1970. The compensated linear vector dipole: a possible mechanism for deep earthquakes, *J. geophys. Res.,* **75,** 4957–4963.

Konstantinou, K.I., 2001. Seismological studies of magma injection processes: volcano monitoring and imaging of magma chambers, *PhD thesis*, University of Durham.

Konstantinou, K.I., 2002. Deterministic nonlinear source processes of volcanic tremor signals accompanying the 1996 Vatnajökull eruption, central Iceland, *Geophys. J. Int.* **148,** 663–675.

Konstantinou, K.I., Nolet, G., Morgan, W.J., Allen, R.M. & Pritchard, M.J., 2000. Seismic phenomena associated with the 1996 Vatnajökull eruption, central Iceland, *J. Volc. Geotherm. Res.,* **102,** 169–187.

Langston, C.A., Barker, J.S. & Pavlin, G.B., 1982. Point source inversion techniques, *Phys. Earth planet. Inter.,* **30,** 228–241.

McNutt, S.R., 1996. Seismic monitoring and eruption forecasting of volcanoes: a review of the state-of-the-art and case histories, in *Monitoring and Mitigation of Volcanic Hazards,* pp. 100–146, ed. Scarpa, T. Springer, Heidelberg.

Menke, W., 1989. *Geophysical Data Analysis: Discrete Inverse Theory*, Academic Press, New York.

Müller, G., 2001. Volume change of seismic sources from moment tensors, *Bull. seism. Soc. Am.,* **91,** 880–884.

Nettles, M. & Ekström, G., 1998. Faulting mechanism of anomalous earthquakes near Bárdarbunga volcano, Iceland, *J. geophys. Res.,* **103,** 17 973–17 983.

Oura, A., Yoshida, S. & Kudo, K., 1992. Rupture process of the Ito-Oki, Japan, earthquake of 1989 July 9 and interpretation as a trigger of volcanic eruption, *Geophys. J. Int.* **109,** 241–248.

Parfitt, E.A., Wilson, L. & Head, J.W., 1993. Basaltic magma reservoirs: factors controlling their rupture characteristics and evolution, *J. Volc. Geotherm. Res.,* **55,** 1–14.

Philpotts, A.R., 1990. *Principles of Igneous and Metamorphic Petrology,* Prentice Hall, Englewood Cliffs.

Press, W., Teukolsky, S.A., Vetterling, W.T. & Flannery, B.P., 1992. *Numerical Recipies in C,* Cambridge University Press, Cambridge.

Priestly, K.F., Brune, J.N. & Anderson, J.G., 1985. Surface wave excitation and source mechanisms of the Mammoth Lakes earthquake sequence, *J. geophys. Res.,* **90,** 11 177–11 185.

Randall, G.E., 1994. Efficient calculation of complete differential seismograms for laterally homogeneous earth models, *Geophys. J. Int.* **118,** 245–254.

Sipkin, S.A., 1986. Interpretation of non-double-couple earthquake mechanisms derived from moment tensor inversion, *J. geophys. Res.,* **91,** 531–547.

Smith, R.P., Jackson, S.M. & Hackett, W.R., 1996. Paleoseismology and seismic hazard evaluations in extensional volcanic terrains, *J. geophys. Res.,* **101,** 6277–6292.

Sugioka, H., Fukao, Y., Kanazawa, T. & Kanjo, K., 2000. Volcanic events associated with an enigmatic submarine earthquake, *Geophys. J. Int.* **142,** 361–370.

Takeo, M., 1992. The rupture process of the 1989 offshore Ito earthquakes preceding a submarine volcanic eruption, *J. geophys. Res.,* **97,** 6613–6627.

Ukawa, M. & Ohtake, M., 1987. A monochromatic earthquake suggesting deep-seated magmatic activity beneath the Izu-Oshima volcano, Japan, *J. geophys. Res.,* **92,** 12 649–12 663.

Wallace, T.C., 1985. A reexamination of the moment tensor solutions of the 1980 Mammoth Lakes earthquakes, *J. geophys. Res.,* **90,** 11 171–11 176.

Walter, W.R. & Brune, J.N., 1993. Spectra of seismic radiation from a tensile crack, *J. geophys. Res.,* **98,** 4449–4459.

Wells, D.L. & Coppersmith, K.J., 1994. New empirical relationships among magnitude, rupture length, rupture width, rupture area and surface displacement, *Bull. seism. Soc. Am.,* **84,** 974–1002.

Zobin, V.M., 1999. The fault nature of the $M_s$ 5.4 volcanic earthquake preceding the 1996 subglacial eruption of Grimsvötn volcano, Iceland, *J. Volc. Geotherm. Res.,* **92,** 349–358.

Zobin, V.M., 2001. Seismic hazard of volcanic activity, *J. Volc. Geotherm. Res.,* **112,** 1–14.

Zobin, V.M. & Levina, V.I., 1998. Rupture history of the January 1, 1996, $M_s$ 6.6 volcanic earthquake preceding the simultaneous eruption of Karimsky and Academia Nauk volcanoes in Kamchatka, Russia, *J. geophys. Res.,* **103,** 18 315–18 324.